

Characteristics of Bose-Einstein condensation in an optical lattice

G.-D. Lin, Wei Zhang, and L.-M. Duan
*FOCUS Center and MCTP, Department of Physics,
University of Michigan, Ann Arbor, Michigan 48109, USA*
(Dated: November 6, 2018)

We discuss several possible experimental signatures of the Bose-Einstein condensation (BEC) transition for an ultracold Bose gas in an inhomogeneous optical lattice. Based on the commonly used time-of-flight imaging technique, we show that the momentum-space density profile in the first Brillouin zone, supplemented by the visibility of interference patterns, provides valuable information about the system. In particular, by crossing the BEC transition temperature, the appearance of a clear bimodal structure sets a qualitative and universal signature of this phase transition. Furthermore, the momentum distribution can also be applied to extract the condensate fraction, which may serve as a promising thermometer in such a system.

PACS numbers: 03.75.Lm, 03.75.Hh, 03.75.Gg

I. INTRODUCTION

There has been significant interest in ultracold atomic gases in optical lattices, partly stimulated by the possibility of simulating strongly correlated many-body systems [1]. With extraordinary controllability, ultracold atomic gases in lattices provide a promising experimental platform to help tackling many important problems in multidisciplinary fields. Among these topics, the emergence of condensation and superfluid order in an optical lattice, and how the superfluid order transforms into other ordered states, is a problem which catches great attention over the past decade. With current technology, condensation and superfluidity are obtained for both Bose and Fermi gases in optical lattices, so that various phase transitions can be investigated [2, 3].

To experimentally investigate these phase transitions, present techniques with ultracold atomic gases heavily rely on detection based on the time-of-flight imaging, where the interference pattern and its visibility are suggested to be signatures of Bose condensation within an optical lattice [2]. Recent studies show that even for a thermal lattice gas above the BEC transition temperature T_c , interference peaks with observable visibility are still present [4, 5, 6]. This thermal visibility can be large for an ideal Bose gas in a homogeneous lattice, which could make the condensation signal ambiguous [4]. However, for practical systems with atomic interaction and an inhomogeneous global trap, the thermal visibility becomes significantly smaller [5, 6], and the appearance of sharp interference peaks is still associated with the BEC transition. It is also suggested that the bimodal structure of the atomic momentum distribution in the first Brillouin zone, combined with the interference peaks, provides an additional unambiguous signal for the Bose condensation in an optical lattice [6]. A very recent experiment has used the onset of the bi-modal distribution and the associated condensate fraction to identify the superfluid-to-Mott-insulator transition point [7].

In this manuscript, we provide a detailed study of a Bose gas in a three-dimensional (3D) inhomogeneous op-

tical lattice, both below and above the BEC transition temperature. We discuss several properties including the visibility, the width of the interference peak, and the momentum distribution of the resulting interference pattern. The main results are as follows. First, all the quantities mentioned above can characterize the BEC transition for the experimental systems with interacting atoms in an inhomogeneous optical lattice. The large thermal visibility applies only to some particular parameters which are not directly responsible for current experiments. In the case when the thermal visibility is large, a substantial variation of the peak width or the appearance of a bimodal structure for the atomic momentum distribution may work as a better signature for the condensation transition. Second, below the BEC transition temperature, the visibility and the peak width become insensitive to the system temperature, hence can not be applied as a practical thermometer. To fulfill this gap, the bimodal structure of the atomic momentum distribution gives a way to extract the condensate fraction through the bimodal fitting. The resulting condensate fraction provides a sensitive indicator of the system temperature, hence may serve as a potential thermometer for this important system.

The calculation techniques in this paper are similar to what we present in Ref. [6]. The remainder of this manuscript is organized as follows. In Sec. II, we first consider the situation of free bosons in an optical lattice within a global harmonic trap, and investigate the general behavior of the interference visibility and the atomic momentum distribution. In the absence of interaction, the problem is significantly simplified such that exact solutions are available. These exact solutions, on the one hand, are valuable for qualitative understanding of the system and its properties, and on the other hand, could be directly compared with experiments when the Feshbach resonance technique is applied to turn off the atomic interaction. After studying the free Bose gas, we then extend our discussion in Sec. III to the case of interacting bosons, where effects of the global harmonic trap and the interaction have to be taken into account together. In or-

der to deal with the trap, we adapt the local density approximation (LDA), which works well when the interaction energy scale is significantly larger than the trapping energy scale (this condition is typically valid for current experiments). Restricting our discussion to weakly interacting bosons that are away from the Mott region, we apply the Hartree-Fock-Bogoliubov-Popov (HFBP) approximation to deal with the atomic interaction [11, 12, 13]. The HFBP method can provide a reliable description except for a narrow region around the BEC transition temperature [11, 14]. Taking into account the effect of the global trap, this questionable region only corresponds to a thin shell in three dimensions and its influence to the global properties is small. Therefore, we expect that the HFBP method can give reliable results for the atomic momentum distribution and the condensate fraction.

II. IDEAL BOSE GAS IN AN INHOMOGENEOUS OPTICAL LATTICE

In this section, we discuss an ideal Bose gas in an inhomogeneous optical lattice with a global harmonic trap. For completeness, we briefly review the formalism [6] before presenting various calculation results. We consider the atoms in a cubic lattice with an additional spherically symmetric harmonic trap [15]. The Hamiltonian takes the form

$$H = \int d^3\mathbf{r} \Psi^\dagger(\mathbf{r}) \left[-\frac{\hbar^2 \nabla_{\mathbf{r}}^2}{2m} + V_{\text{op}}(\mathbf{r}) + V(\mathbf{r}) \right] \Psi(\mathbf{r}), \quad (1)$$

where Ψ represents the bosonic field operator, m is the atomic mass, $V_{\text{op}}(\mathbf{r}) \equiv V_0 \sum_{i=x,y,z} \sin^2(\pi r_i/d)$ is the optical lattice potential with lattice spacing d , and $V(\mathbf{r}) \equiv m\omega^2 r^2/2$ is the global harmonic trapping potential. In practice, the global harmonic trap $V(\mathbf{r})$ typically varies much slower than the optical lattice potential $V_{\text{op}}(\mathbf{r})$, so the Hamiltonian can be separated into two parts with fast and slow variations, respectively. The fast-varying part can be diagonalized by introducing the expansion of bosonic field operators

$$\Psi(\mathbf{r}) = \sum_{\mathbf{R}} w(\mathbf{r} - \mathbf{R}) a_{\mathbf{R}}, \quad (2)$$

where $w(\mathbf{r})$ is the Wannier function associated with the lattice potential $V_{\text{op}}(\mathbf{r})$, $a_{\mathbf{R}}$ is the annihilation operator on site \mathbf{R} , and the summation is over all lattice sites. After transforming to the momentum space, the Fourier components of $\Psi(\mathbf{r})$, $w(\mathbf{r})$, and $a_{\mathbf{R}}$ satisfy the following relation

$$\Psi(\mathbf{k}) = w(\mathbf{k}) a_{\mathbf{k}}. \quad (3)$$

Representing the fast and slow varying components of H in terms of $a_{\mathbf{k}}$ and $a_{\mathbf{R}}$, respectively, the original Hamiltonian Eq. (1) can be written as

$$H = \sum_{\mathbf{k} \in 1\text{BZ}} \epsilon_{\mathbf{k}} a_{\mathbf{k}}^\dagger a_{\mathbf{k}} + \sum_{\mathbf{R}} V(\mathbf{R}) a_{\mathbf{R}}^\dagger a_{\mathbf{R}}, \quad (4)$$

where the summation over quasi-momentum \mathbf{k} is restricted to the first Brillouin zone (1BZ). Here, we assume that the lattice depth V_0 is strong enough such that the band gap is large and atoms are confined to the lowest band with dispersion relation $\epsilon_{\mathbf{k}} = -2t \sum_{i=x,y,z} \cos(k_i d)$. The tunneling rate t can be well estimated by $t \approx (3.5/\sqrt{\pi}) V_0^{3/4} \exp(-2\sqrt{V_0})$, where the recoil energy $E_{\text{R}} \equiv \hbar^2 \pi^2 / (2md^2)$ is used as the energy unit [16].

In principle, the resulting Hamiltonian Eq. (4) can be directly diagonalized for arbitrary $V(\mathbf{R})$. However, the numerical calculation is usually very heavy in three dimensions due to the presence of a large number of lattice sites. In this case, the diagonalization process can be significantly simplified by noticing that the indices \mathbf{k} and \mathbf{R} in Eq. (4) are reminiscent of the coordinate and the momentum variables in quantum mechanics. This observation allows us to write down a first quantization Hamiltonian corresponding to Eq. (4) in the momentum space, where \mathbf{R} is replaced by the momentum gradient $-i\nabla_{\mathbf{k}}$ [6, 8, 9, 10]. The resulting effective Hamiltonian thus takes the form

$$H_{\text{eff}} = -\frac{1}{2} m\omega^2 \nabla_{\mathbf{k}}^2 + \epsilon_{\mathbf{k}}, \quad (5)$$

which represents free bosons with effective mass $m^* \equiv \hbar^2 / (m\omega^2)$ in a periodic potential $\epsilon_{\mathbf{k}}$ with period $|\mathbf{G}| = 2\pi/d$ along all three principal directions. Furthermore, since $\nabla_{\mathbf{k}}^2$ and $\epsilon_{\mathbf{k}}$ are separable, this Hamiltonian can be reduced to three one-dimensional problems which require much less effort to solve. Notice that the properties of this effective Hamiltonian depend only on the ratio of $\hbar^2 \omega^2 / (tE_{\text{R}})$, which suggests that the variation of ω and V_0 can be scaled to each other by fixing the dimensionless parameter $\hbar^2 \omega^2 / (V_0^{3/4} e^{-2\sqrt{V_0}})$, where E_{R} is used as the energy unit. In this section, we will keep V_0 fixed ($V_0 = 10E_{\text{R}}$) and look at changes of the system properties under variation of the global trapping frequency ω . With different lattice barriers V_0 , one can directly read out the result by simply re-scaling ω to keep $\hbar^2 \omega^2 / (V_0^{3/4} e^{-2\sqrt{V_0}})$ fixed (a smaller barrier thus corresponds to a larger effective trapping frequency).

The quasi-momentum distribution $\langle a_{\mathbf{k}}^\dagger a_{\mathbf{k}} \rangle$ is then given by the square of the eigenstate wave functions $\phi_{\mathbf{n}}(\mathbf{k})$ of H_{eff} , where the expectation value is obtained by averaging over all eigenstates \mathbf{n} with a Bose distribution factor $g(E_{\mathbf{n}}) = 1 / \exp[\beta(E_{\mathbf{n}} - \mu) - 1]$. Here, $E_{\mathbf{n}}$ is the corresponding eigenenergy, μ is the chemical potential, and $\beta = 1/(k_{\text{B}}T)$ is the inverse temperature. Taking into account the presence of the Wannier function in Eq. (3), the atomic *real* momentum distribution is

$$\begin{aligned} n(\mathbf{k}) &= \langle \Psi^\dagger(\mathbf{k}) \Psi(\mathbf{k}) \rangle = |w(\mathbf{k})|^2 \langle a_{\mathbf{k}}^\dagger a_{\mathbf{k}} \rangle \\ &= |w(\mathbf{k})|^2 \sum_{\mathbf{n}} g(E_{\mathbf{n}}) |\phi_{\mathbf{n}}(\mathbf{k})|^2. \end{aligned} \quad (6)$$

For a free gas, this momentum distribution remains unchanged during expansion, so that the signal from the

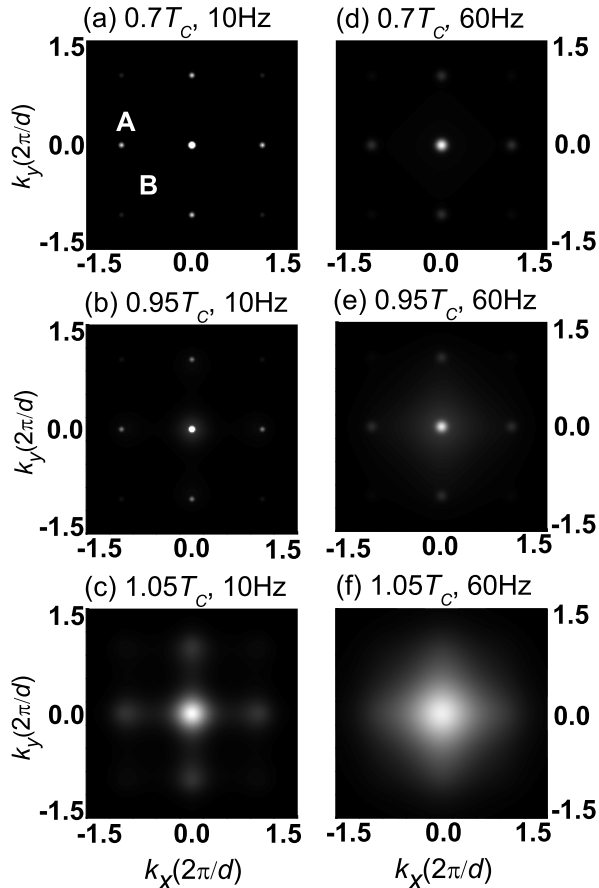


FIG. 1: Calculated column-integrated momentum density profile near the first Brillouin zone measured through the time-of-flight imaging, taking for two different trapping frequencies at various temperatures. Parameters chosen in these plots are close to those for a typical experiment of ^{87}Rb , with lattice depth $V_0 = 10E_R$ and a total number of particles $N = 10^5$. The global harmonic trapping frequencies are $\omega = 2\pi \times 10$ Hz for (a)-(c), and $2\pi \times 60$ Hz for (d)-(f).

time-of-flight image taking along a crystallographic axis, say z direction, is just the columnar density

$$n_{\perp}(k_x, k_y) = \int n(\mathbf{k}) dk_z. \quad (7)$$

Using the technique sketched above, we show in Fig. 1 the calculation results for the column-integrated momentum distribution as record by the time-of-flight images, both below and above the BEC transition temperature T_c . In these plots, we choose parameters close to those for a typical experiment of ^{87}Rb atoms, where the lattice depth $V_0 = 10E_R$, and the total number of particles $N = 10^5$. For this finite system, the transition temperature T_c is determined by requiring that the number of atoms in the ground state is of the order of 1 when $T > T_c$

and increases by orders of magnitude when T crosses T_c . Since the total atom number satisfies $N \gg 1$, the transition is actually very sharp, and T_c is well defined by the requirement above.

From Fig. 1, one can see that for the case of a very weak global trap ($\omega = 2\pi \times 10$ Hz), the interference peaks are indeed clearly visible even above the transition temperature. However, the BEC transition is still evident from the time-of-flight images as the interference peaks become much sharper when T gets below T_c . For the case with a stronger global trap ($\omega = 2\pi \times 60$ Hz, which is close to the value in experiments), the interference peaks become blurred when $T > T_c$ (although one can still read some pattern). Again, across the transition temperature T_c , the time-of-flight image, in particular the sharpness of the central peak, undergoes a dramatic change.

These figures show that qualitatively a Bose condensation transition should be visible with the time-of-flight images. To have a more quantitative description, however, it is desirable to have some single-value indicators which change sharply across the BEC transition so that one can characterize this phase transition by measuring the indicators. As possible candidates, we next discuss in detail two quantities, including the visibility of the interference pattern and the peak width associated with the atomic momentum distribution in Sec. II A and II B, respectively. While both of the two quantities can signify the BEC transition in a reasonably strong global trap, the peak width becomes more accurate when the global trap gets weaker. After the condensation transition, both of these two indicators become very insensitive to the variation of the system temperature, so they do not provide a good thermometer. Instead, we suggest to measure the condensate fraction from the bimodal fitting to the central interference peak, as discussed in Sec. II C. The measured condensate fraction change continuously with the temperature, thus gives a good indicator for estimation of temperature in this important system.

A. Visibility of the interference pattern

The visibility of the interference pattern has been introduced in Ref. [17]. It is defined as the intensity contrast of two characteristic points on the interference pattern [17]

$$v = \frac{n_{\perp}^A - n_{\perp}^B}{n_{\perp}^A + n_{\perp}^B}, \quad (8)$$

where n_{\perp}^A and n_{\perp}^B are (column-integrated) atomic intensities at sites A and B , respectively, as shown in Fig. 1(a). The point A represents the position of the secondary peak while B is along the circle of the secondary peaks where the intensity takes its minimum. The visibility defined in this way is clearly independent of the Wannier function [the pre-factor in Eq. (3)].

The temperature dependence of the visibility v , especially by crossing the BEC transition, is shown in Fig. 2

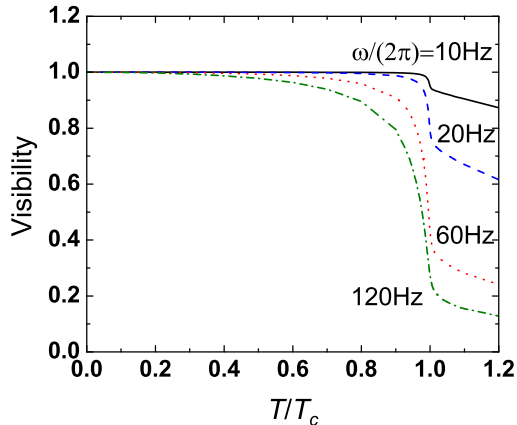


FIG. 2: (color online) The visibility as a function of temperature around the BEC transition temperature T_c for various values of trapping frequencies. Other parameters are the same as those used in Fig. 1 with $V_0 = 10E_R$ and $N = 10^5$. Remind that the variation of V_0 is equivalent to that of ω , with a fixed value of $\hbar^2\omega^2/(V_0^{3/4}e^{-2\sqrt{V_0}})$.

for various values of trapping frequencies. For a very weak trap ($\omega = 2\pi \times 10$ Hz), the visibility is pretty high ($v > 0.8$) even with the temperature considerably larger than T_c . So in the limit of a vanishing ω , this is consistent with the results in Ref. [4] for free bosons in a homogeneous lattice (without the global trap). However, for large trapping frequencies, as pointed out in Ref. [5], the visibility becomes significantly smaller when $T > T_c$, leading to a more substantial drop across the BEC transition. With a trapping frequency around $\omega = 2\pi \times 60$ Hz, the visibility jumps should be pretty evident to observe, as shown in Fig. 2. However, the transition is stretched over a wide range of temperatures (the visibility begins to drop starting from a temperature significantly below T_c , see Fig. 2), which may make the determination of the transition point from the visibility less accurate. Notice that with the scaling relation, a smaller barrier V_0 corresponds to a larger effective trapping frequency ω . So with a shallower lattice, the change in the visibility across the BEC transition gets larger for free bosons.

For the system temperature above T_c , there is no long range coherence in the atomic cloud, so the finite visibility of the interference pattern is induced by residue short-range thermal correlations. To understand the different behavior of the visibility, we calculate the short-range thermal correlation function around the trap center with different global trapping potentials. The real space correlation function is defined as

$$C(\mathbf{R}) = \frac{\langle \Psi^\dagger(\mathbf{0})\Psi(\mathbf{R}) \rangle}{\sqrt{\langle \Psi^\dagger(\mathbf{0})\Psi(\mathbf{0}) \rangle \langle \Psi^\dagger(\mathbf{R})\Psi(\mathbf{R}) \rangle}}, \quad (9)$$

with $\mathbf{R} = \mathbf{0}$ indicating the trap center. In Fig. 3, we show the correlation functions both below and above T_c

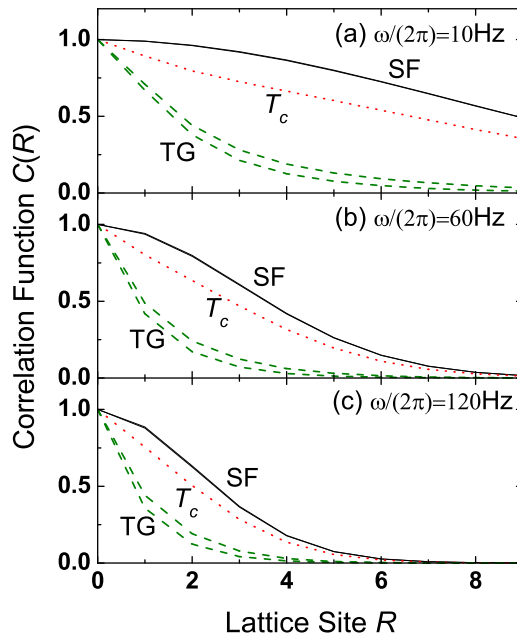


FIG. 3: (color online) Correlation functions around the trap center indicating real space coherence below (for a superfluid, SF) and above (for a thermal gas, TG) the BEC transition temperature, with trapping frequencies (a) $\omega = 2\pi \times 10$ Hz, (b) $2\pi \times 60$ Hz, and (c) $2\pi \times 120$ Hz. Curves in each panel are taken at, from top to bottom, $0.9T_c$ (solid), $0.95T_c$ (solid), $1.0T_c$ (dotted), $1.05T_c$ (dashed), and $1.1T_c$ (dashed), respectively. Parameters used in these plots are $V_0 = 10E_R$ and $N = 10^5$. For reference, the characteristic length of the single particle ground state wavefunction adjusted by effective mass ($L \equiv \sqrt{\hbar/m^*\omega}$) are (a) $L = 23.1$, (b) $L = 9.4$, and (c) $L = 6.7$, respectively.

for different trapping frequencies. Notice that for weak trapping potentials [see, e.g., Fig. 3(a)], the correlation function extends to several lattice sites at temperatures above T_c , indicating the presence of thermal short-range coherence. As the trapping frequency increases, the correlation length for a thermal gas decreases as presented in Fig. 3(b) and 3(c), which is consistent with the disappearance of interference peaks as shown in Fig. 2(f).

B. Momentum-space density profile and the peak width

Up to now, we discuss the visibility characterizing the contrast of the interference pattern. In this subsec-

tion, we introduce another single-value quantity, the peak width, which characterizes the sharpness of the interference peak. We notice that while the visibility does not undergoes a sudden change across the BEC transition when the global trap is weak, the width of the central interference peak, however, always shrinks sharply when the condensation takes place. Therefore, the peak width is always a good indicator of the BEC transition independent of the strength of the global trap

To introduce the peak width, first we look at the atomic momentum distribution, which gives more detailed information about the system. From Eq. (3), the momentum distributions in other Brillouin zones are simply copies of the distribution in the first Brillouin zone weighted by the given Wannier function, so it suffices to study the atomic momentum profile in the first Brillouin zone. In Fig. 4, we plot the column-integrated momentum distribution along one crystallographic axis (e.g., the x -axis) passing through the center of the first Brillouin zone. It is clear that while the density profile is a thermal distribution when $T > T_c$, a bimodal structure starts to appear when a non-zero condensate fraction emerges in the lattice, characterized by a sharp peak at the center of the momentum space surrounded by a flat thermal distribution. The signal of this structural change is significant as soon as the system crosses the BEC transition [see Fig. 4(b) and (e)].

In order to characterize the sharpness of the atomic momentum distribution in the first Brillouin zone, we introduce the peak width as a single-value parameter. For this purpose, we first define the middle value of $n_{\perp}(k_x, k_y)$ within the first Brillouin zone

$$n_{\text{mid}} \equiv \frac{1}{2} \left[\max_{(k_x, k_y) \in \text{1BZ}} + \min_{(k_x, k_y) \in \text{1BZ}} \right] n_{\perp}(k_x, k_y). \quad (10)$$

In the simplest term, the peak width w is measured as the radius in the momentum space where the (column-integrated) atomic density $n_{\perp}(k_x, k_y)$ first falls to this middle value n_{mid} . In Fig. 5, we show the peak width as a function of temperatures for various trapping frequencies. Notice that the central peak width decreases monotonically with temperature, and most importantly, undergoes a sharp and substantial change by crossing the transition temperature. This distinctive feature is universal for all trapping frequencies, hence can provide a clear criterion for the phase transition. However, as will be discussed later, the sharpness of the change of central peak width around T_c is guaranteed only for ideal Bose gases. In the presence of atomic interaction, the variation of central peak width may be more flat and extended over a wider range of temperatures.

C. The condensate fraction as a measure of temperature

From the discussion above, we notice that after the condensation transition, both the visibility and the peak

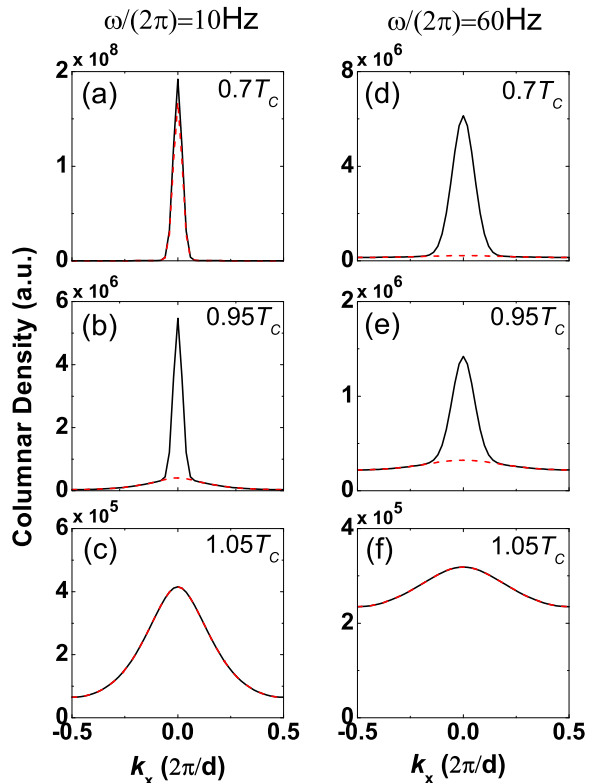


FIG. 4: (color online) Momentum space columnar density along the x -axis in the first Brillouin zone. The left and right panels correspond to the cases of trapping frequencies $\omega = 2\pi \times 10\text{Hz}$ and $2\pi \times 60\text{Hz}$, respectively. Notice that while a thermal distribution is present above T_c [(c) and (f)], a clear bimodal structure starts to appear for temperatures slightly below T_c with only precentral condensate fractions [$n_0 \sim 0.14$ in (b) and ~ 0.09 in (e)]. Here, the solid curves represent the total momentum density profile, and the dashed curves represent the momentum density profile of the normal component. Parameters used in these plots are $V_0 = 10E_R$ and $N = 10^5$.

width become almost flat to variation of temperature, as one can see from Figs. 2 and 5. This means that it is hard to get any information about the temperature of the system from the measured values of visibility and peak width. Since temperature is one of the most important quantity for the thermodynamical property of the system, it is desirable to have some experimentally measurable indicator which gives a good estimate of the temperature. The momentum density profile in principle gives a lot of information, but it is not a single-value quantity which makes it hard to support a direct comparison at different temperatures or for different systems. To overcome this drawback, we note that below T_c , the atomic momentum distribution in the first Brillouin zone always shows a bimodal structure, which actually gives a universal signal for the condensation transition. Further-

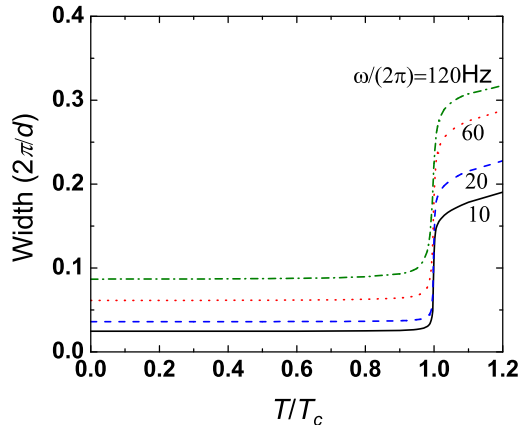


FIG. 5: (color online) The peak width (defined in the text) within the first Brillouin zone, taking across the transition temperature for various values of trapping frequencies. Notice that the sharp and substantial change around T_c occurs for all cases hence serves as a distinctive signature of BEC transition. Parameters used in these plots are $V_0 = 10E_R$ and $N = 10^5$.

more, from the measured momentum density profile, one can always do a bimodal fitting to figure out the atomic fractions in the condensate and in the thermal parts, respectively. The measured condensate fraction thus can serve as a good estimate for the system temperature. In Fig. 6, we show the calculated condensate fraction as a function of temperature for this system with two different global trapping frequencies. Notice that the condensate fraction n_0 changes steadily and monotonically as the temperature T varies. From the relation $n_0(T)$, one can estimate the temperature T through the experimentally measurable n_0 . Therefore, the condensate fraction n_0 gives a single-value quantity which can serve as a criterion for the condensation transition (with $n_0 > 0$), as well as an indicator of the system temperature.

III. INTERACTING BOSE GAS IN AN INHOMOGENEOUS OPTICAL LATTICE

In this section, we discuss the more general and practical case where the atoms in an inhomogeneous optical lattice has collisional interactions with each other. Many qualitative features discussed in the last section, however, remain valid in the interacting case. The atomic interaction indeed brings up several different properties in a quantitative level. In this section, the emphasis of our discussion is on these differences.

By taking the interaction into account, the time-of-flight images are expected to be modified in two major aspects. First, the repulsive interaction between atoms will tend to broaden their spatial distribution in a trap, and hence narrow the corresponding momentum distribution. Second, during the time-of-flight expansion, the remnant

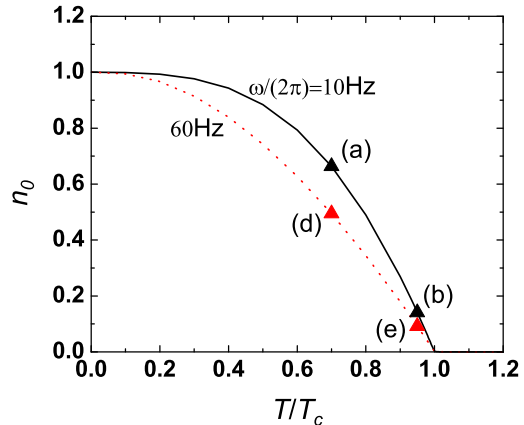


FIG. 6: (color online) The condensate fraction as a function of temperature below the BEC transition. By extracting n_0 from the momentum distribution as shown in Fig. 4(a-b) and (d-e), temperatures of such cases can be determined correspondingly (triangles). Parameters used in this figure are $V_0 = 10E_R$ and $N = 10^5$.

atomic interaction transforms the interaction energy into the kinetic energy, in particular in the early stage of expansion. As a consequence, the momentum distribution tends to be wider in the final images. The images also get a bit blurred due to the scattering of different interference peaks in the momentum space during the expansion. In this section, we will discuss both of these two points.

For an interacting Bose gas in an inhomogeneous optical lattice, exact solutions as in the non-interacting case no longer exist. Instead, we use the local density approximation (LDA) to treat the inhomogeneity induced by the global trap. When the interaction energy is much larger than the trap energy, each local region of the global trap behaves like a homogeneous system with interacting atoms in a pure optical lattice. The interaction in this local homogeneous lattice is then analyzed under the Hartree-Fock-Bogoliubov-Popov (HFBP) scheme [11, 14]. The validity of this approach is supported by the following considerations. First, the LDA works well for a large number of atoms in a weak harmonic trap, which is the case for the parameter ranges considered below. Second, the HFBP method should be able to provide a reliable description of weakly interacting Bose systems, except for the region close to a phase transition (associated with the BEC or the Mott transition). For an atomic gas in a global harmonic trap away from the Mott transition, such questionable region corresponds only to a thin shell in space, and its contribution to the global properties is far less significant.

Under the LDA, we consider an interacting Bose system with a spatially dependent Hamiltonian

$$H = \sum_{\mathbf{k}} (\epsilon_{\mathbf{k}} - \mu) a_{\mathbf{k}}^{\dagger} a_{\mathbf{k}} + \frac{U}{2} \sum_{\mathbf{k}, \mathbf{k}', \mathbf{q}} a_{\mathbf{k}+\mathbf{q}}^{\dagger} a_{-\mathbf{k}}^{\dagger} a_{\mathbf{k}'+\mathbf{q}} a_{-\mathbf{k}'}, \quad (11)$$

where $\epsilon_{\mathbf{k}}$ is the dispersion relation defined above, $\mu \equiv \mu(\mathbf{r})$ is the local chemical potential, and $U \equiv U_{\text{bg}} \int |w(\mathbf{r})|^4 d^3\mathbf{r}$ is the on-site interaction rate. For a typical experiment of ^{87}Rb , U_{bg} is related to the s -wave background scattering length $a_s = 5.45$ nm by $U_{\text{bg}} = 4\pi\hbar^2 a_s/m$, and U takes an approximate form of $U \approx 3.05V_0^{0.85}(a_s/d)$, with an energy unit of the recoil energy E_R [17]. With the standard HFBP approach, we separate the bosonic operators into two parts:

$$a_{\mathbf{k}} = \psi_0 + \delta_{\mathbf{k}}; \quad a_{\mathbf{k}}^\dagger = \psi_0 + \delta_{\mathbf{k}}^\dagger, \quad (12)$$

where $\psi_0 \equiv \langle a_0^\dagger \rangle \equiv \langle a_0 \rangle$ represents the condensate component, and $\delta_{\mathbf{k}}$ is the fluctuation around it. After performing the substitution for $a_{\mathbf{k}}$ and $a_{\mathbf{k}}^\dagger$ into the original Hamiltonian Eq. (11), terms that are cubic and quartic in $\delta_{\mathbf{k}}^\dagger$ and $\delta_{\mathbf{k}}$ will be present. These terms are reduced to quadratic forms under the HFBP by employing the Wick's theorem. As a result, we obtain a quadratic effective Hamiltonian H_{eff}

$$\begin{aligned} H_{\text{eff}} \approx & \left(\epsilon_0 - \mu + \frac{Un_0}{2} \right) n_0 \\ & + \sum_{\mathbf{k}} [\epsilon_{\mathbf{k}} - \mu + 2U(n_{\text{tot}} - n_0)] \delta_{\mathbf{k}}^\dagger \delta_{\mathbf{k}} \\ & + \frac{Un_0}{2} \sum_{\mathbf{k}} \left(\delta_{\mathbf{k}}^\dagger \delta_{-\mathbf{k}}^\dagger + \delta_{\mathbf{k}} \delta_{-\mathbf{k}} + 4\delta_{\mathbf{k}}^\dagger \delta_{\mathbf{k}} \right). \end{aligned} \quad (13)$$

Here, $\epsilon_0 = -6t$ is the energy at the band bottom with t is the tunnelling rate defined above, $n_0 = \psi_0^2$ is the per site density of the condensate fraction, and n_{tot} is the total number of particles per site. In order to derive the expression above, the saddle point condition is employed to make the coefficients of terms linear in δ vanish, leading to the saddle point equation

$$\mu(\mathbf{r}) = \epsilon_0 - Un_0 + 2Un_{\text{tot}}. \quad (14)$$

This equation must be solved self-consistently with the number constraint $n_{\text{tot}} = -\partial\Omega/\partial\mu$, where $\Omega = -(1/\beta) \ln \text{Tr}(e^{\beta H_{\text{eff}}})$ is the thermodynamical potential. This constraint leads to the number equation

$$n_{\text{tot}} = n_0 + \sum_{\mathbf{k} \neq 0} \frac{1}{2} \left[\frac{\epsilon_{\mathbf{k}} - \epsilon_0 + Un_0}{E_{\mathbf{k}}} \coth \left(\frac{\beta E_{\mathbf{k}}}{2} \right) - 1 \right], \quad (15)$$

where $E_{\mathbf{k}} = \sqrt{(\epsilon_{\mathbf{k}} - \epsilon_0 + Un_0)^2 - U^2 n_0^2}$ is the quasiparticle dispersion relation.

By fixing the number density per site at the trap center, we can solve Eqs. (14) and (15) self-consistently to obtain the chemical potential at the trap center μ_0 . This result, together with the LDA relation of $\mu(\mathbf{r}) = \mu_0 - V(\mathbf{r})$, allows us to calculate $\mu(\mathbf{r})$, and hence the condensate fraction $n_0(\mathbf{r})$ and quasi-momentum distribution of the non-condensate part $n_{\mathbf{k} \neq 0}(\mathbf{r})$ at arbitrary position in the trap. The overall non-condensate quasi-momentum distribution, thus can be obtained by integrating over the whole global trap. For the condensate

component, it should be emphasized that n_0 leads to a delta function at zero momentum, which is an artificial result of LDA. In order to overcome this artifact, one needs to consider explicitly the broadening of the condensate momentum distribution due to the presence of the harmonic trap. This can be done by the following procedure. First, we get the condensate fraction distribution $n_0(\mathbf{r})$ over the trap. The condensate wave function then can be well approximated by $\psi_0(\mathbf{r}) = \sqrt{n_0(\mathbf{r})}$ under the Thomas-Fermi approximation [18]. The condensate component of the quasi-momentum distribution is thus given by the Fourier transform of the wave function $\psi_0(\mathbf{r})$. Second, by adding this condensate contribution to that from the normal part, and multiplied by the Wannier function square $|w(\mathbf{k})|^2$ as in Eq. (6), we get the resulting momentum-space density distribution.

Next, as in the case of an ideal Bose gas, we discuss several characteristics on the momentum-space density distribution. In Sec. III A and III B, we discuss the influence of interaction on the atomic momentum distribution inside the trap, especially the associated visibility and the peak width, respectively. Then, we calculate in Sec. III C the condensate fraction as a quantitative measure of the system temperature. Lastly, in Sec. III D, we analyze the interaction effect during the time-of-flight expansion, and conclude that this effect does not change much the characteristics discussed above.

A. Visibility of the interference pattern

We show in Fig. 7 the visibility of the interference pattern as a function of temperature across the BEC transition. Since the presence of interaction sets another energy scale, the system is not determined by the single parameter of $\hbar^2\omega^2/(tE_R)$, as in the ideal gas case. Instead, we consider various combinations of lattice barriers and trapping frequencies.

From Fig. 7(a), we find that independent of the strength of the global trap, the thermal visibility with $T \gtrsim T_c$ remains small (with v about or below 0.4). This result is significantly different from the case of an ideal Bose gas, where the thermal visibility can be close to the unity for a very weak global trap. By crossing the BEC transition, the visibility clearly increases so that for an interacting Bose gas, a high visibility signifies that the atomic cloud is in the condensate region. However, for a strong global trap (with $\omega \sim 2\pi \times 120$ Hz for instance), the variation of the visibility is not sharp at the transition point, but continues into a pretty wide region below T_c . Thus, in this case, it becomes less accurate to use the jump of the visibility to determine the BEC transition temperature.

Another feature we can read from Fig. 7(a) is the convergent behavior of visibility for a thermal gas with the same lattice potential but various values of trapping frequency. This behavior can be understood from the over-

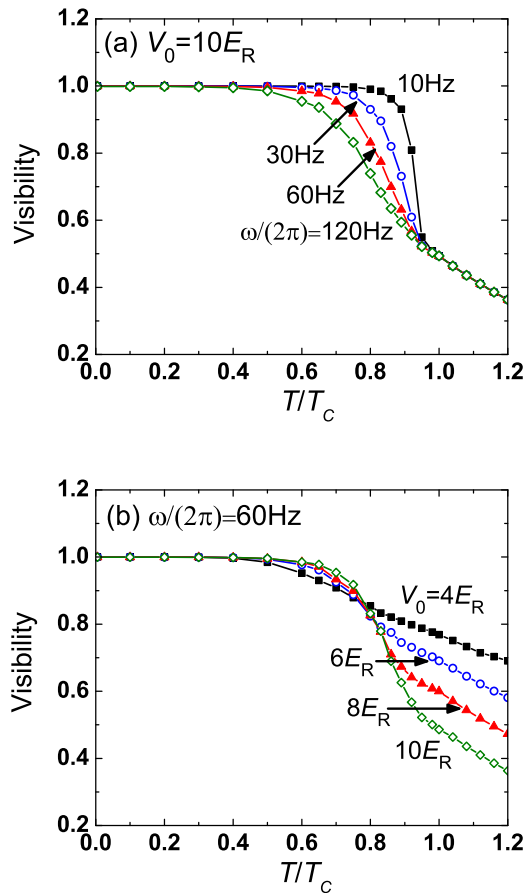


FIG. 7: (color online) The visibility as a function of temperature around the BEC transition temperature T_c for (a) $V_0 = 10E_R$ and (b) $\omega = 2\pi \times 60$ Hz. The number density per site at the trap center is set as $n_{\text{tot}} = 1$, and the total number of particles in the trap is $N \sim 10^4$.

all quasi-momentum distribution

$$n_{\mathbf{k}} = \int d^3\mathbf{r} n_{\mathbf{k}}(\mathbf{r}) = 4\pi \int_0^\infty dr n_{\mathbf{k}}(r) r^2, \quad (16)$$

where the integration is over the whole trap. Under the LDA, the spatial dependence of number density is only through the chemical potential $n_{\mathbf{k}}(\mathbf{r}) = \tilde{n}_{\mathbf{k}}(\mu(\mathbf{r}))$, hence the integration can be rewritten as

$$n_{\mathbf{k}} = 4\pi \left(\frac{m}{2\omega^2}\right)^{3/2} \int_{\mu_0}^0 \varepsilon \tilde{n}_{\mathbf{k}}(\varepsilon) d\sqrt{\varepsilon}. \quad (17)$$

For a thermal gas with a certain number density and chemical potential at the trap center, the function $\tilde{n}_{\mathbf{k}}(\varepsilon)$, and hence the integration over ε in the equation above is fixed. Thus, all the trap can do is to re-scale the quasi-momentum distribution by a factor of ω^{-3} . For a given optical lattice characterized by a Wannier function, the momentum-space density profile of a thermal gas for var-

ious values of ω takes the identical shape, hence all signatures we can read from it must remain the same. Notice that since the LDA approach is reliable for all parameter ranges discussed here (with $\omega \lesssim 2\pi \times 120$ Hz), we conclude that this result is the effect of a strong interaction compared to the trapping potential, which can not be smoothly connected to the non-interacting results.

In Fig. 7(b), we show the visibility for different lattice depths with a fixed strength of the global trap. With lower lattice depths, the thermal visibility increases. For $V_0 = 4E_R$, for instance, the visibility varies almost linearly with temperature near the condensation transition (for T from $0.5T_c$ to $1.2T_c$), and a high thermal visibility remains (with $v \sim 0.7 - 0.8$) even when T crosses T_c . This flat behavior hence makes it difficult to use visibility to signify the condensate region and to identify the transition point for interacting atoms in a shallow lattice.

B. Momentum-space density profile and the peak width

After discussing the visibility of interference peaks, we next focus on the momentum distribution in the first Brillouin zone. In Fig. 8, we show the column-integrated momentum density profile along one of the crystallographic axis (say, the x -axis). Similar to the case of an ideal Bose gas, a clear bimodal structure appears for temperatures below T_c even when the condensate fraction is still small [see Fig. 8(b) with $n_0 \sim 9\%$]. Therefore, the momentum distribution and its bimodal structure sets an unambiguous criterion for the BEC transition, especially when supplemented with the interference pattern from the lattice structure.

To characterize the sharpness of the central peak, we still use the peak width defined above as a single-value parameter. As shown in Fig. 9, the peak width significantly reduces across the BEC transition, so a sharp peak with a small width sets a clear indicator that the system is in the condensate region. This conclusion is qualitatively consistent with the case of an ideal Bose gas as discussed in Sec. II B. For an ideal Bose gas, the peak width always has a sharp and large jump at the BEC transition point. For an interacting Bose gas, this jump becomes less sharp under certain circumstances. From Fig. 9, we notice that the jump of the peak width remains sharp across T_c for weak global traps or for lower lattice depths. However, in a stronger global trap with a higher lattice depth, the decrease of the peak width takes place over a wider range of temperatures, which makes it less accurate to locate the transition point using the peak width as an indicator. If one compares Figs. 7 and 9, it is interesting to note for that for a weak optical lattice, even when the visibility becomes too flat to show a phase transition, the variation of the peak width remains significant and sharp to serve as an indicator of the condensation transition.

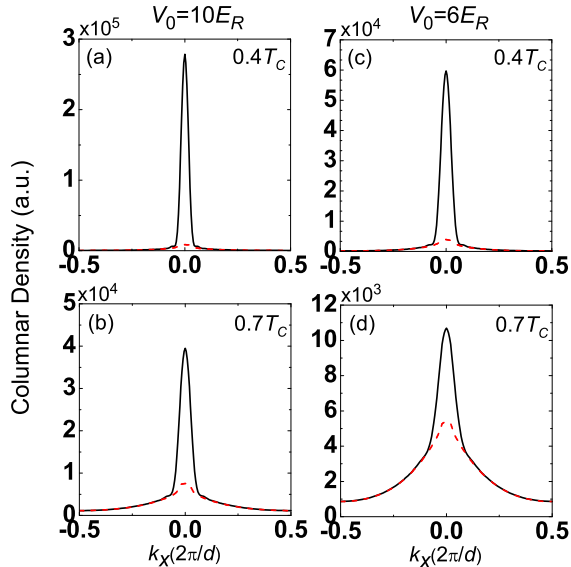


FIG. 8: (color online) Momentum space columnar density along the x -axis in the first Brillouin zone, where clear bimodal structures appear for temperatures below T_c . Here, the solid curves are the total momentum density profile, and the dashed curves are the momentum density profile of the normal component. The trapping frequency used in these plots is $\omega = 2\pi \times 60$ Hz, and the number density per site is unity at the trap center.

C. The condensate fraction

As in the case of an ideal Bose gas, when one moves into the condensate region, the visibility and the peak width become insensitive to the variation of temperature. Instead, we need to use the condensate fraction as an indicator of the temperature in the condensate region. The condensate fraction can be measured similarly through the bimodal fitting to the atomic momentum distribution. In Fig. 10, we show the total condensate fraction as a function of the temperature under a couple of different lattice barriers. First, the condensate fraction change monotonically and sensitively with temperature, so it provides a potentially good thermometer. Second, it is interesting to note that the condensate fraction does not approach the unity even when the temperature tends to zero. This result is significantly different from the case of an ideal Bose gas, where at zero temperature it is always a pure condensate. This discrepancy is due to quantum depletion of the condensate at zero temperature, which is always present for an interacting gas. In the zero temperature limit, the HFBP approximation used here reduces to the Bogoliubov approach, so it naturally takes into account the contribution from quantum depletion. In Fig. 11, we show the in-trap zero temperature quantum depletion fraction for various lattice barrier depths. Notice that by applying a higher lat-

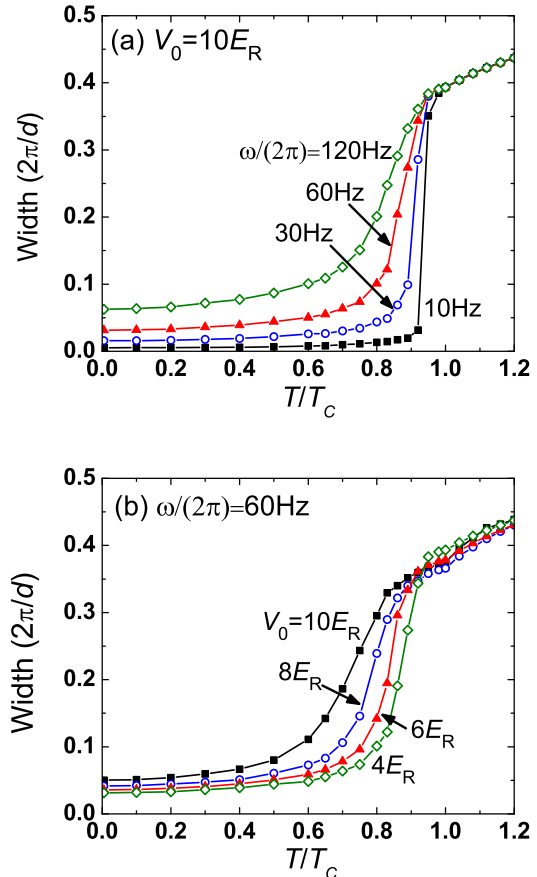


FIG. 9: (color online) The peak width within the first Brillouin zone, taking across the transition temperature for (a) $V_0 = 10E_R$ and (b) $\omega = 2\pi \times 60$ Hz. The number density per site is unity at the trap center.

tice barrier V_0 , the quantum depletion fraction gets more significant. This observation justifies the zero temperature results of condensate fraction as shown in Fig. 10, and is consistent with the trend one should expect. In fact, in the case with no optical lattice, the condensate fraction should approach unity at zero temperature for a weakly interacting dilute gas (with a small gas parameter). In the opposite limit, when the lattice barrier tends to the critical value for the Mott transition, the condensate fraction should deplete to zero. When the quantum depletion is dramatic, the HFBP is no longer a good approximation. However, for parameter ranges discussed above, even with $V_0 = 12E_R$, the condensate fraction ($\sim 70\%$) still dominates at zero temperature, assuring the validity of the HFBP approximation used throughout this section.

Another interesting feature of the condensate fraction plot Fig. 10 is the crossing behavior of the two curves for different V_0 at finite temperature. For a homogeneous gas with a certain number density, one would expect a more

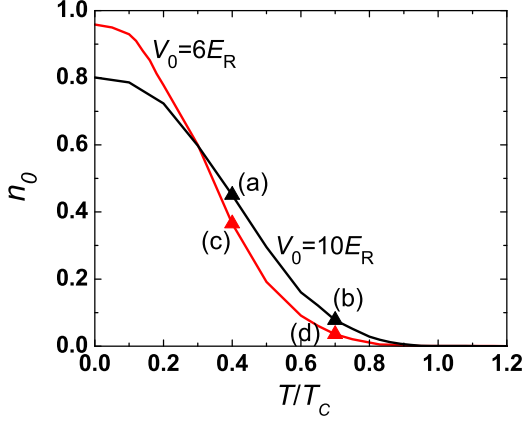


FIG. 10: (color online) The condensate fraction as a function of temperature below the BEC transition, for an interacting Bose gas in an optical lattice with $\omega = 2\pi \times 60$ Hz and different lattice barriers V_0 . The number density per site is unity at the trap center. By comparing with the momentum distribution as shown in Fig. 8, temperatures of such a system can be determined correspondingly (triangles).

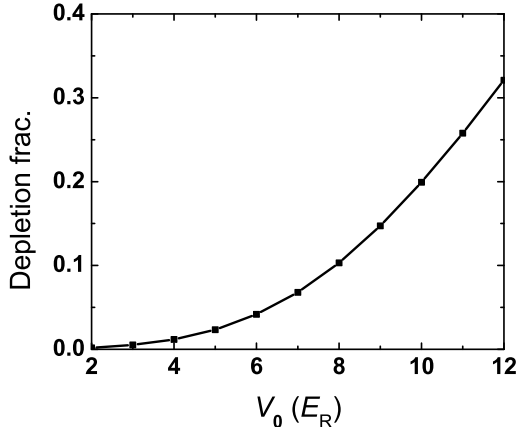


FIG. 11: The in-trap quantum depletion fraction as a function of the lattice barrier V_0 . The trapping frequency is $\omega = 2\pi \times 60$ Hz. The number density per site at the trap center is unity.

severe depletion (both quantum and thermal) from the condensate for the higher V_0 case, since both temperature and interaction would play relatively more significant role when the transfer integral t decreases. However, this simple trend becomes more complicated in a trapped case. In fact, due to the presence of a global trap, thermal wings must emerge at the edge at any finite temperature. As one calculate the in-trap condensate fraction, an integration over the whole trap should take the thermal wings into account, and the result will inevitably

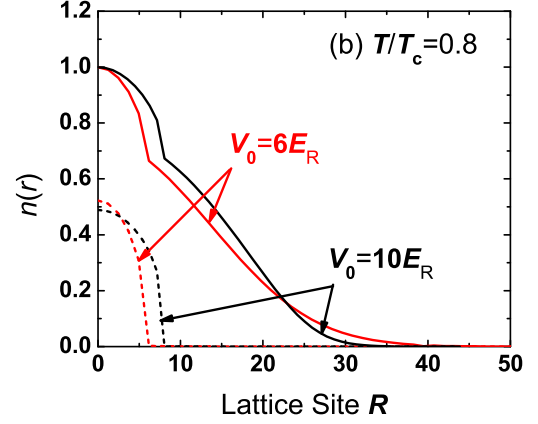
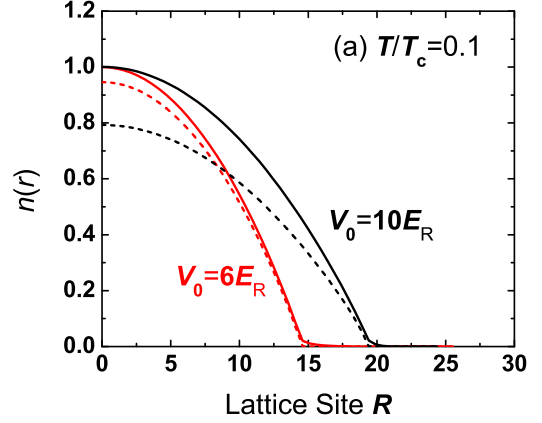


FIG. 12: (color online) The number and condensate density distribution along the radial direction away from the trap center. Two different temperatures are considered as in (a) $T = 0.1T_c$, and (b) $T = 0.8T_c$. The solid curves correspond to the overall density profiles and the dashed curves to the condensate portions. The trapping frequency used here is $\omega = 2\pi \times 60$ Hz. The total number of particles N_{tot} and the number of condensate particles N_0 are respectively (a) $V_0 = 6E_R$ (red): $N_{\text{tot}} = 0.54 \times 10^4$, $N_0 = 0.50 \times 10^4$; $V_0 = 10E_R$ (black): $N_{\text{tot}} = 1.3 \times 10^4$, $N_0 = 1.0 \times 10^4$; (b) $V_0 = 6E_R$ (red): $N_{\text{tot}} = 2.5 \times 10^4$, $N_0 = 2.8 \times 10^2$; $V_0 = 10E_R$ (black): $N_{\text{tot}} = 2.3 \times 10^4$, $N_0 = 6.7 \times 10^2$.

depend on how much the thermal part contribute to the total number. As an example, we show the in-trap number and condensate density profiles in Fig. 12 with fixed total number density at the trap center. At a lower temperature $T = 0.1T_c$, the thermal contribution is negligible so it is apparent that a higher depletion is observed in higher barriers, as shown in Fig. 12(a). At a higher temperature $T = 0.8T_c$, the thermal part becomes significant and one observes a more extended thermal tail in the lower barrier case with $V_0 = 6E_R$, as shown in Fig. 12(b). This greater thermal contribution to the total number makes the condensate part relatively smaller and leads to a smaller condensate fraction. Therefore,

the crossing behavior of n_0 as shown in Fig. 10 is a consequence of the inhomogeneous distribution of different phases with various number density and chemical potential, which are results from the inhomogeneity of the trap.

D. Interaction effects during the time-of-flight expansion

Up to now, we have calculated the atomic momentum distribution inside the trap and have neglected modification of this distribution caused by the atomic interaction during the time-of-flight expansion. During the expansion of the atomic cloud, the initial interaction energy is transferred to the kinetic energy, which tends to broaden the momentum distribution [19]. This influence is most evident for the condensate part, due to its high number density and narrow momentum distribution at the beginning. The influence on the momentum distribution of the thermal and the non-condensate part is negligible, as confirmed by experiments [5], since this part has a broad initial momentum distribution already, and the weak atomic collisions are unlikely to cause any significant modification. In the following, we only discuss influence of the atomic collisions on the condensate part of the momentum distribution.

After turnoff of the optical lattice and the confining potential, the atomic cloud undergoes a free expansion in space, and the expansion of the condensate part can be well described by a time dependent Gross-Pitaevskii (TDGP) equation

$$i\hbar\partial_t\Psi(\mathbf{r},t) = \left(-\frac{\hbar^2\nabla_{\mathbf{r}}^2}{2m} + U|\Psi(\mathbf{r},t)|^2\right)\Psi(\mathbf{r},t), \quad (18)$$

where the initial condition $\Psi(\mathbf{r},t=0)$ (t is the expansion time) is given by the equilibrium condensate wave function inside the optical lattice and global trap, which has been calculated with the method detailed in the above. Note that only for the condensate part we use the TDGP to evolve its momentum distribution.

It is easier to understand the consequence of this evolution by looking at the TDGP equation in the momentum space. The Fourier transform of Eq. (18) gives

$$i\hbar\partial_t\Psi_{\mathbf{k}}(t) = \frac{\hbar^2k^2}{2m}\Psi_{\mathbf{k}}(t) + U\sum_{\mathbf{k}',\mathbf{q}}\Psi_{-\mathbf{k}+\mathbf{q}}^\dagger(t)\Psi_{-\mathbf{k}'+\mathbf{q}}(t)\Psi_{\mathbf{k}'}(t). \quad (19)$$

Clearly, without atomic collisions (the U term), the momentum distribution $|\Psi_{\mathbf{k}}(t)|^2$ remains unchanged. The atomic collisions transfer a pair of atoms from momenta $(\mathbf{k}', -\mathbf{k}'+\mathbf{q})$ to $(\mathbf{k}, -\mathbf{k}+\mathbf{q})$, which modulates the overall momentum distribution.

To understand the consequence of the collision induced momentum transfer, we note that the initial condensate momentum distribution has a number of peaks, one in

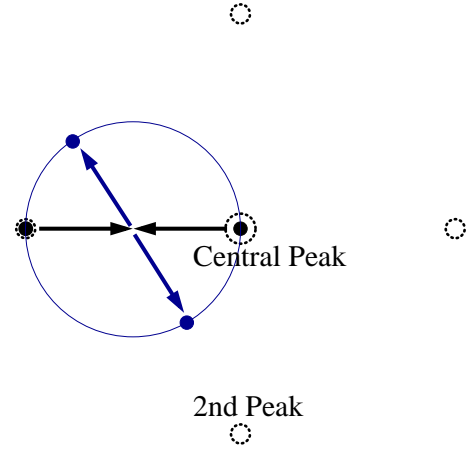


FIG. 13: Illustration of the scattering between atoms from different peaks (the central and the secondary). This process leads to blurring of the interference peaks with a characteristic blurring pattern.

each Brillouin zone. As the central peak in the first Brillouin zone (with \mathbf{k} close to zero) is the highest one, the scattering of pairs of atoms around the first peak satisfying the momentum conservation has the largest contribution to the collision effect. Around the central peak, the wave function $\Psi_{\mathbf{k}}(t)$ has approximate spherical symmetry, and the evolution of the momentum distribution around the central peak by the TDGP equation has been calculated and shown in Ref. [6]. The condensate peak gets somewhat lower and broader, however, its width is typically still significantly less than the width of the thermal cloud, and a bimodal structure of the momentum distribution remains clearly visible. Thus, the collision during the time-of-flight expansion has some quantitative influence on the peak width we calculate before, but the effect is not large and it should not change all the qualitative discussions in the last sections. In particular, as the bimodal structure remains clearly observable, we do not expect that the condensate fraction measured through the bimodal fitting to the momentum distribution has any significant change by the collision effect during the expansion.

In the next order, the atom in the central peak can collide with another atom in the secondary peak, and scatter to some other directions in the momentum space. The momentum difference between the central peak and the secondary peak is given by \mathbf{G} (\mathbf{G} is related to the lattice constant d through $|\mathbf{G}| = 2\pi/d$), so the kinetic energy difference between them corresponds to a large energy scale $\hbar^2|\mathbf{G}|^2/(2m)$, which is typically larger than the interaction strength during the expansion [the latter can be estimated by $Un(t)$, where $n(t)$ is the instantaneous atomic density at the collision]. Therefore, to be effective, the collisions need to satisfy the momentum conservation as well as an approximate energy conservation in the momentum space. As a consequence, for atoms

with incoming momenta around 0 and G (corresponding to the central and the secondary peaks, respectively), the outgoing atoms are centered around a spherical surface in the momentum space as shown in Fig. 13 [with momenta $(\mathbf{k}', -\mathbf{k}' + \mathbf{G})$, where $\mathbf{k}'^2 + (-\mathbf{k}' + \mathbf{G})^2 \approx |\mathbf{G}|^2$]. The sphere has origin at $\mathbf{k} = \mathbf{G}/2$ and a radius of $|\mathbf{G}|/2$. This collision effect causes some blurring of the original peaks. Since the scattered atoms are dominantly around a sphere in the momentum space, this blurring scattering gives some characteristic momentum distribution pattern. Experimentally, by looking at such a pattern, one may measure and constraint the magnitude of collision effects during the time-of-flight expansion.

At high orders, there could be also scattering between different secondary peaks as well as scattering between the central and even higher order peaks. Although these scattering can change some of quantities we calculate before, we expect all these modifications are pretty small.

IV. CONCLUSION

In summary, we have discussed in this manuscript ideal as well as interacting Bose gases in an inhomogeneous optical lattice within a global harmonic trap. By explicitly calculating the momentum distribution, we have studied several possible signatures of the BEC transition in a lattice based on the common detection technique of time-of-flight imaging. For parameters of relevance to the

current experiments, a large visibility, a substantial decline of the peak width, and the appearance of a bimodal structure for the central peak, can all be used as signals of the condensation transition as one decreases the temperature. For some other parameters, the thermal visibility could be significant, and in such a case the latter two criteria will work better. In particular, the appearance of a bimodal structure for the momentum distribution is a robust signal associated with the condensation transition in both free space and lattice (in the lattice case, the interference peaks give further information about the underlying lattice structure).

After the condensation transition, both the visibility and the peak width become insensitive to the variation of temperature, so they can not serve as a practical thermometer. Instead, one may measure the condensate fraction by a bimodal fitting to the atomic momentum distribution. The condensate fraction changes steadily with temperature, and may work as a good experimental indicator of the system temperature by comparing with the results from theoretical calculations.

Acknowledgments

We thank Immanuel Bloch for helpful discussions. This work is supported under ARO Award W911NF0710576 with funds from the DARPA OLE Program and the MURI program.

-
- [1] For a review, see I. Bloch and M. Greiner, *Adv. At. Mol. Opt. Phys.* **53**, 1 (2005).
 - [2] M. Greiner, O. Mandel, T. Esslinger, T. W. Hänsch, and I. Bloch, *Nature* **415**, 39 (2002).
 - [3] J. K. Chin, D. E. Miller, Y. Liu, C. Stan, W. Setiawan, C. Sanner, K. Xu, W. Ketterle, *Nature* **443**, 961 (2006).
 - [4] R. B. Diener, Q. Zhou, H. Zhai, and T.-L. Ho, *Phys. Rev. Lett.* **98**, 180404 (2007).
 - [5] F. Berber, S. Fölling, A. Widera, and I. Bloch, eprint arXiv: cond-mat/0701420, (2007).
 - [6] W. Yi, G.-D. Lin, and L.-M. Duan, *Phys. Rev. A* **76**, 031602(R) (2007).
 - [7] I. B. Spielman, W. D. Phillips, and J. V. Porto, (to be published).
 - [8] A. Polkovnikov, S. Sachdev, and S. M. Girvin, *Phys. Rev. A* **66**, 053607 (2002).
 - [9] C. Hooley and J. Quintanilla, *Phys. Rev. Lett.* **93**, 080404 (2004).
 - [10] A. M. Rey, G. Pupillo, C. W. Clark, and C. J. Williams, *Phys. Rev. A* **72**, 033616 (2005).
 - [11] J. O. Andersen, *Rev. Mod. Phys.* **76**, 599 (2004).
 - [12] D. van Oosten, P. van der Straten, and H. T. C. Stoof, *Phys. Rev. A* **63**, 053601 (2001).
 - [13] A. M. Rey, K. Burnett, R. Roth, M. Edwards, C. J. Williams, and C. W. Clark, *J. Phys. B* **36**, 825 (2003).
 - [14] H. Shi and A. Griffin, *Phys. Rep.* **304**, 1 (1998).
 - [15] The cases of different lattice structures and anisotropic trapping potentials can be analyzed analogously, provided that the anisotropy of the global trap is not strong enough to cause a breakdown of LDA.
 - [16] L.-M. Duan, *Phys. Rev. Lett.* **95**, 243202 (2005).
 - [17] F. Gerbier, A. Widera, S. Fölling, O. Mandel, T. Gericke, and I. Bloch., *Phys. Rev. Lett.* **95**, 050404 (2005).
 - [18] F. Dalfovo, S. Giorgini, L. P. Pitaevskii, and S. Stringari, *Rev. Mod. Phys.* **71**, 463 (1999).
 - [19] In this paper, we have assumed that the expansion time is long enough so that the final absorption image represents the initial momentum distribution (the far-field limit). In real experiments, the expansion time may be not long enough to achieve this far-field limit (I. Bloch, private communication). This leads to some effective momentum broadening effect seen in observation, which looks similar to the momentum broadening caused by the atomic interaction. However, these two effects should be distinguished. According to the calculation here, the interaction induced momentum broadening is actually not significant for a condensate with a moderate density (such as about one atom per site). The effective broadening effect seen in observation caused by the finite expansion time in principle can be undone theoretically if one knows the initial condensate profile and the expansion time.